



Pyrrolic nitrogen-doped carbon sandwiched monolayer MoS₂ vertically anchored on graphene oxide for high-performance sodium-ion battery anodes

Xiaoxuan Ma¹ · Na Li¹ · Shikun Liu¹ · Kun Zhang¹ · Caixia Chi¹ · Jiupeng Zhao¹ · Xiaoxu Liu^{1,2} · Yao Li³

Received: 2 March 2018 / Revised: 9 May 2018 / Accepted: 11 May 2018 / Published online: 21 May 2018
© Springer-Verlag GmbH Germany, part of Springer Nature 2018

Abstract

In this work, a novel pyrrolic nitrogen-doped carbon sandwiched monolayer MoS₂ hybrid was prepared. This sandwiched hybrid vertically anchors on graphene oxide as anode materials for sodium-ion batteries. Such electrode was fabricated by facile ionic liquid-assisted reflux and annealing methods. Owing to rational structure and enhancement from pyrrolic nitrogen dopant, this unique MoS₂/C-graphene hybrid exhibits reversible specific capacity of 486 mAh g⁻¹ after 1000 cycles with a low average fading capacity of 0.15 mAh g⁻¹ (fading cyclic rate of ca. 0.03% per cycle). A capacity of 330 mAh g⁻¹ is remained at the current densities of 10.0 A g⁻¹. The proposed strategy provides a convenient way to create new pyrrolic nitrogen-doped hybrids for energy field and other related applications.

Keywords Sandwiched nanoarchitectures · Pyrrolic nitrogen-doped carbon · MoS₂ · Sodium-ion battery

Introduction

The urgent demands for renewable energy storage systems require to develop sodium-ion storage technologies [1, 2]. Sodium-ion batteries (SIBs) are regarded as representative alternatives for replacing the conventional energy sources, owing to their desirable properties of resource abundance and cost-effectiveness [3, 4]. Unremitting efforts from world-

wide scientists are searching appropriate anode materials for achieving high reversibility and long-life SIBs [5]. Despite the similar mechanism with rechargeable lithium-ion batteries (LIBs), SIBs suffer from undesirable durability and limited rate performance [6]. The problems mainly originate from the larger ionic radius of Na⁺ (1.06 Å for Na⁺ via 0.76 Å for Li⁺), leading to serious degradation of the electrodes or sluggish Na⁺ kinetics [7].

Among various potential anode materials, molybdenum disulfide (MoS₂) could be considered as a “shining star,” due to its graphene-like structure [8]. This unique structure is in favor of Na⁺ diffusion kinetics and the conversion reaction (1T-MoS₂ to metal Mo and Na₂S), which could benefit high theoretical capacity (Na⁺ enters the S layer to form Na–S bonds) [9]. Such sodiation/desodiation mechanism results in rapid capacity fading, which derived from (a) aggregation, pulverization, and restack for the nanomaterials (by volume change and mechanical stress); (b) the electrode degradation (arising from sluggish Na⁺ insertion kinetics and poor conductivity); and (c) dissolved loss of sulfur (via soluble Na₂S_n and shuttle effect) [10, 11].

To overcome these obstacles, the synthetic strategies could be mainly divided into three categories: ultrathin MoS₂ nano-sheets, wide-interlayer spacing of MoS₂, and maximizing the MoS₂/carbon contact [12, 13]. Various as-prepared MoS₂-

Electronic supplementary material The online version of this article (<https://doi.org/10.1007/s10008-018-3994-z>) contains supplementary material, which is available to authorized users.

✉ Jiupeng Zhao
jiupengzhao@126.com

✉ Xiaoxu Liu
liu88062321@163.com

✉ Yao Li
yaoli@hit.edu.cn

¹ School of Chemistry and Chemical Engineering, Harbin Institute of Technology, Harbin 150001, People’s Republic of China

² Heilongjiang University of Science and Technology, Harbin 150022, People’s Republic of China

³ Center for Composite Materials and Structure, Harbin Institute of Technology, Harbin 150001, People’s Republic of China

based materials are efficacious to enhance the cycling stability and improve rate capacity [14]. Among these, MoS₂/C sandwiched structure has been attracting attention with the integrated advantages of the above three strategies [15]. Chen and co-workers have synthesized mesoporous carbon sandwiched MoS₂ hollow microspheres by an aerosol spraying pyrolysis method, which displays 390 mAh g⁻¹ after 2500 cycles at 0.1 A g⁻¹ [16]. Xu's group created the carbon sandwiched monolayer MoS₂ assembled hierarchical nanotubes, which delivered a capacity as high as 477 mAh g⁻¹ after 200 cycles at 0.2 A g⁻¹ [17].

Atomic interface contact between MoS₂ and carbon is significant for high-performance anodes for SIBs [18]. Because of large interface contact between MoS₂ and carbon, optimized carbon can well address the key issues on MoS₂-based anode in hybrids [19]. Chen's group synthesized the flower-like MoS₂ by hydrothermal synthesis assisted with an ionic liquid (IL) 1-butyl-3-methylimidazolium tetrafluoroborate [20]. The electrochemical performances of the electrode were significantly enhanced. But there is no evidence to show the carbon or nitrogen-doped carbon composite in the electrode. Zhao's group prepared lamellar structure with MoS₂ layers uniformly decorated on graphene sheets. The direct coupling of edge Mo of MoS₂ with the oxygen from functional groups on graphene oxide (C–O–Mo bond) is proposed [21]. However, they focused on the coupling effect of oxygen on graphene oxide with molybdenum disulfide rather than incorporation of nitrogen atoms. The electrical properties of carbon can be easily improved by the incorporation of nitrogen atoms. The chemical and electronic properties of the carbon host depend on nitrogen doping configurations and nitrogen content [22].

Different from graphitic N and pyridinic N, pyrrolic N not only possesses strong Na–N and S–N attraction but also maintains high electronic conductivity of carbon matrix. However, sandwiched MoS₂/C hybrid with high pyrrolic N content is rarely reported and remains a big challenge [23].

Herein, for the first time, we report a facile synthesis of MoS₂/C-graphene hybrid as high-performance anode for SIBs. In this hybrid, a novel pyrrolic nitrogen-doped carbon sandwiches monolayer MoS₂. And, these sandwiched hybrids vertically anchor on graphene oxide. Unlike previously reported MoS₂-based SIBs, pyrrolic nitrogen-doped carbon have adequately contacted with S atoms from monolayer MoS₂, which endows more active sites and mitigating the polysulfide shutting. The sandwiched structure in the hybrids maximizes the interface contact of MoS₂/C and effective isolates in MoS₂ phase. The electrochemical performance of hybrid anode manifests the reversible specific capacity of 486 mAh g⁻¹ after 1000 cycles with a very low capacity decay of ca. 0.003% per cycle at 0.2 A g⁻¹ (a low average fading capacity of 0.15 mAh g⁻¹ per cycle). A capacity of 330 mAh g⁻¹ is remained at current densities of 10.0 A g⁻¹.

Experimental

All the reagents were purchased from Sigma-Aldrich. The reagents were of analytical grade and were used directly without further purification. We used a modified Hummers method to synthesize graphene oxide. In the process, we put 120 ml concentrated sulfuric acid into a round bottom flask, which was kept at 0 °C using an ice water bath. Then, 1.2 g NaNO₃ and 1.2 g graphite powder (400 mesh) were added slowly while stirring, and 3.0 g KMnO₄ was added into the mixture gradually and reacted for 90 min. The system was then stirred at room temperature for 3 h. Furthermore, 300 ml deionized water was added dropwise to the above solution. After that, 240 ml deionized water and 32 ml 30% H₂O₂ were slowly added at room temperature sequentially. We used deionized water and 5% hydrochloric acid to wash the obtained product three times. Finally, the product was freeze-dried to obtain graphene oxide powder.

In a typical procedure, 3.0 mmol 1-ethyl-3-methylimidazolium chloride ([EMIm]Cl) was dispersed into 15 ml deionized water. The 10 ml graphene oxide (GO) aqueous dispersion (0.12 mg l⁻¹) was added dropwise to resultant solution with vigorous stirring. The mixture was stirred for an additional 2 h at room temperature, which can make the positive-charged [EMIm]⁺ well absorbed on the negative-charged GO surface. Then, 30 ml oleylamine and 10 mmol (NH₄)₂MoS₄ were added and sonicated for 20 min to form a uniform dispersion. The reaction mixture was heated for 60 min at reflux conditions at 360 °C under N₂. Finally, the samples denoted as MGH obtained after annealed at 600 °C for 2 h in Ar atmosphere. For comparison, the composite sample was also prepared by a similar route except the use of [EMIm]Cl or GO, which named MG and ME.

Material characterizations

Scanning electron microscopy (SEM) performed on Hitachi S-4800 was used to characterize the morphology of as-synthesized hybrids. Transmission electron microscopic (TEM), high-resolution transmission electron microscopic (HRTEM) images, and energy dispersive X-ray spectra (EDS) were recorded by using a JEOL JEM-2010 microscope. Zetasizer 3000HS was used to characterize the surface zeta potential of the hybrids. The Raman spectrum was achieved using a WITec CRM 200 confocal system with a laser wavelength of 550 nm. The crystallographic information of the samples was investigated by powder X-ray diffraction (XRD), which were collected with a Max-2500 with non-monochromatic Cu-K α radiation in a 2 θ range from 5° to 80° at room temperature. X-ray photoelectron spectroscopy (XPS) characterization was recorded on a PHI-5000 Versaprobe instrument with a monochromatized Al K α X-

ray source (1486.6 eV) scanning a spot size of 700 by 300 μm , and the mass of the samples is 8.5 mg. The carbon content analyses in the hybrids were determined by thermogravimetric (TGA) analysis on PerkinElmer Pyris 6 TG Analyzer in air atmosphere at a raising rate of 5 $^{\circ}\text{C min}^{-1}$ from 25 to 800 $^{\circ}\text{C}$, and the mass of the samples is 7.5 mg.

Electrochemical measurements

The electrochemical properties were evaluated by assembly of two-electrode 2016 coin cells in a glove box filled with pure Ar gas. The working electrodes on the Al foils were composed of the as-prepared hybrids, conductive carbon black, and binders in a weight ratio of 70:20:10 by slurring in *N*-methylpyrrolidone. In sodium half cells, metallic sodium foil was used as the counter-electrode. The electrolyte used was 1.0 M NaPF_6 in ethylene carbonate/diethyl-carbonate/fluoroethylene carbonate (EC/DEC/FEC) (1:1:0.05 v/v). The separator used was glass fiber (GF/D), and the binder was polyvinylidene fluoride (PVDF). The active material loading mass was about 2.0–2.5 mg cm^{-2} . The galvanostatic charge/discharge cycling behavior was tested on a multichannel NEWARE BTS-610 battery testing system (Newware Technology Co. Ltd., China) at room temperature. Cyclic voltammetry (CV) curves were performed in a CHI660E electrochemical workstation (Shanghai Chenhua Co. Ltd., China) at a scan rate of 0.2 mV s^{-1} .

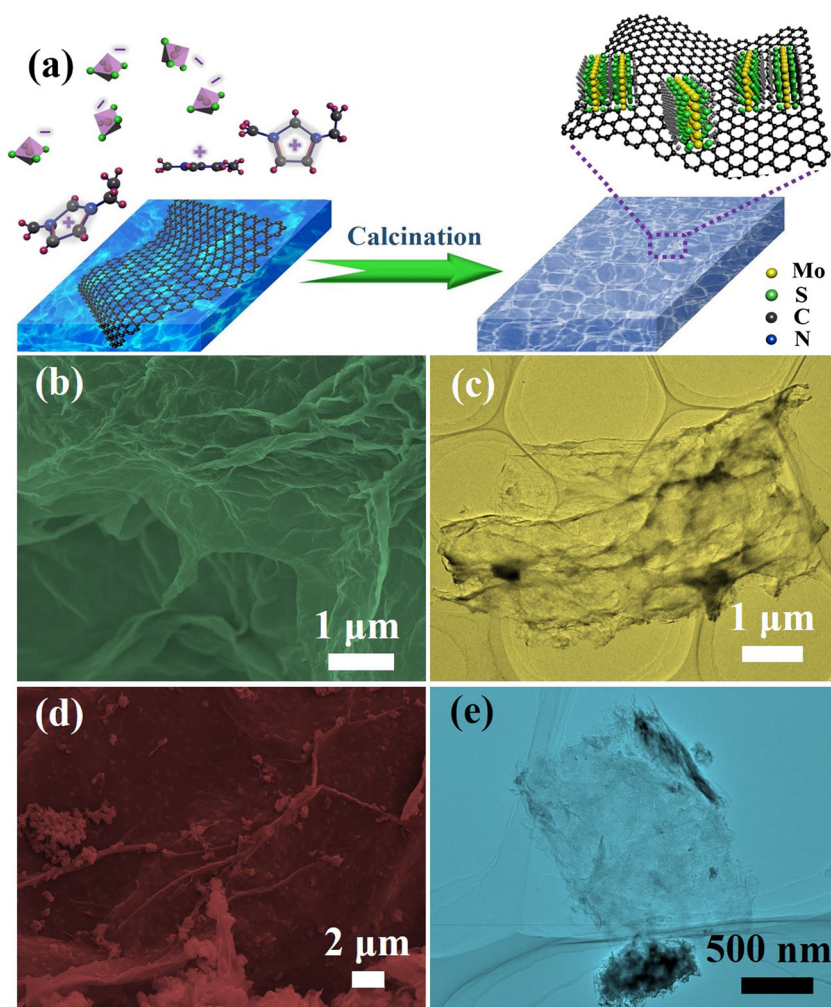
Results and discussions

Figure 1a graphically illustrates the fabrication protocol of MGH. Briefly, the MGH precursor was obtained by $[\text{EMIm}]\text{Cl}$ -assisted reflux method. Electrostatic attraction attracts the positive-charged $[\text{EMIm}]^+$ ion on the negative-charged GO surface. Subsequently, negative-charged MoS_4^{2-} mixes with $[\text{EMIm}]^+$ ion subsequently hybrid on the modified GO surface. After annealing, the hybrids were successfully obtained. The highly pyrrolic nitrogen-doped carbon derived from the pyrolysis imidazole group. The morphology of the samples was identified by SEM and TEM. As shown in Fig. 1b, c, MGH exhibits curved thin flaky structure and wrinkled surface, indicating the hybrids successfully homogeneously encapsulated on the GO surface. Such attachment to flexible and stable GO surfaces can mitigate the fracture and pulverization of MoS_2 , achieving high reversible capacity of the electrode. MoS_2 particles separated from GO show that electrostatic repulsion makes the MoS_2 isolated growth without the $[\text{EMIm}]\text{Cl}$ assisted (Fig. 1d). The SEM and TEM images of the ME are presented in Fig. S1a and b. Totally different from wrinkled and sheet-like appearance, the ME shows particle-like morphology without GO addition.

The EDX spectrum discloses the presence of C, N, Mo, and S elements in this hybrid (Fig. 2a). The obvious N signal in MGH implies highly doped nitrogen proportion in carbon matrix. It can be obviously found the monolayer MoS_2 and super wide-interlayer spacing MoS_2 in HRTEM image (Fig. 2b). The lattice spacing of MoS_2 is sufficiently expanded to ca. 0.99–1.44 nm (much larger than 0.62 nm of bulk MoS_2). Line profiles of the d-spacing of the MoS_2 interlayers reveal the existence of carbon layers between the adjacent MoS_2 layers (Fig. 2c). Agreement with the calculated results, the interlayer spacing of 0.99 nm presents the insertion of carbon monolayer and 1.38 nm exhibits the insertion of two carbon layers [24]. The carbon layer sandwiched MoS_2 is suggested to be vital for maintaining adequate S–C hetero-interface and reasonable isolated MoS_2 phase in the long-term cycles [25]. The EDX elemental mappings further confirmed the complete coverage of MoS_2/C hybrids on GO with homogeneous spatial distributions of C, N, Mo, and S. As observed in Fig. 2d–h, the EDX spectra of MG show the existence of C, Mo, and S elements without N element in Fig. 2i. Mo and S signals disappear on the surface of GO, and the C signal does not appear in MoS_2 nanoparticle. As observed, it further demonstrates separation of MoS_2 and GO without $[\text{EMIm}]^+$. Figure 2j shows the HRTEM image of MG, displaying typical “graphene-like” MoS_2 layers. And, the line profiles over MoS_2 interlayers of MG reveal multilayer structure with interlayer spacings of 0.635 nm in Fig. 2k. HRTEM images of ME show the high crystalline nature of the MoS_2 layers and thin carbon film uniformly coated on MoS_2 nanoparticle (Fig. S1c).

The zeta potential measurement was performed to explore the assisted function of $[\text{EMIm}]^+$ ions (Fig. 3a). Assisted by $[\text{EMIm}]^+$, ions adsorbed on the GO surface the zeta potential from negative-charged -28.6 mV to positive-charged 22.4 mV. Electrostatic attraction is dominant in the adsorption of MoS_4^{2-} groups mixed with residual $[\text{EMIm}]^+$ ion subsequently. After annealing, zeta potential of the as-prepared hybrid is -25.6 mV, resulting the existence of negative surface charge MoS_2 . However, zeta potential of MGH is lower than related literature information, indicating less exposition of surface sulfur atoms, which are consistent with vertically sandwiched MoS_2 monolayer structure in HRTEM images [26]. The crystallographic information of as-obtained electrodes is investigated by XRD in Fig. 3b. All the diffraction peaks match well with the pure phase of standard hexagonal 2H- MoS_2 structure (JCPDS No. 37-1492), except diffraction peaks located at 26° ascribed to N-doped carbon and GO [25]. Compared with MG and ME, MGH exhibits a weaker and broader (002) diffraction ranging from 5.5° to 12.3° with a wider d-spacing of 0.78–1.60 nm. The results reveal the more disordered arrangement of S–Mo–S layers and the enlarged interlayer spacing between neighboring MoS_2 layers, which is in good agreement with the HRTEM observation.

Fig. 1 **a** Schematic illustration for the fabrication of MoS₂ electrodes. **b** SEM images of MGH. **c** TEM image of MGH. **d** SEM images of MG. **e** TEM image of MG



The Raman spectroscopy characterization verifies coexistence of MoS₂ and C in Fig. S2. The significant characteristic peaks of D (1375) band and G (1592) band of carbon imply the disorderly stacked carbon with N incorporation derived from imidazole derivatives. Figure 3c highlights the presence of MoS₂-related peaks corresponding to in-plane (E_{2g}^1) and out-of-plane (A_{1g}) vibration mode [27]. As the two characteristic peaks of MoS₂ are sensitive to intra-layer bonding and molecule interaction, one of the prominent indicators for MoS₂ layers is the frequency difference (Δ) between the two peaks [28]. The Raman peaks of ME and MG appear at 409.1 nm^{-1} (A_{1g}) and 383.4 nm^{-1} (E_{2g}^1) with the value of Δ estimated to be 25.7 cm^{-1} . In comparison with ME and MG, E_{2g}^1 peak of MGH shows a red shift and A_{1g} peak exhibits a blue shift, suggesting that interlayer coupling increased interlayer Van der Waals force and structural strain dominated the change of vibration [29]. This Δ value is measured to be 20.7 nm^{-1} , supporting the presence of single-layer MoS₂ ($20.2\text{--}21.2 \text{ cm}^{-1}$ of MoS₂ single layer). When comparing the intensity ratio ($I_{E_{2g}^1}/I_{A_{1g}}$) of the three electrodes, this ratio for MGH (0.26) is much lower than those of ME (0.46) and

MG (0.48). The difference verifies that MGE belong to edge-terminated and vertically aligned [30]. Such vertical edge-terminated structure with the enlarged MoS₂ basal planes can facilitate electrical conductivity, shorten Na⁺ diffusion paths, and migrate soluble polysulfide intermediate shuttling [31].

The corresponding high-resolved XPS spectra of Mo and S would be interpreted into two doublets. Observation from the two characteristic peaks located at 232.5 and 229.3 eV, assigned to Mo 3d_{5/2} and Mo 3d_{3/2}, demonstrates the presence of Mo⁴⁺ in Fig. 3d. The binding energies of spin-orbit doublet of S 2p_{3/2} and S 2p_{1/2} are 162.1 and 163.3 eV, showing the existence of S²⁻ (Fig. 3e). The atomic percentages of MGH are Mo of 29.82, S of 59.41, C of 8.29, N of 0.83, and O of 1.75 at%. The stoichiometric ratio of S and Mo can be estimated to be nearly 1.99 based on the peak area, approaching the theoretical value of MoS₂. The C1s peaks at 284.7 eV, ascribed to C–C/C=C, confirms that amorphous carbon was formed in the as-prepared samples (Fig. S2). Nitrogen-bonding configurations in the carbon were then quantitatively analyzed by high-resolution XPS measurements detailed in

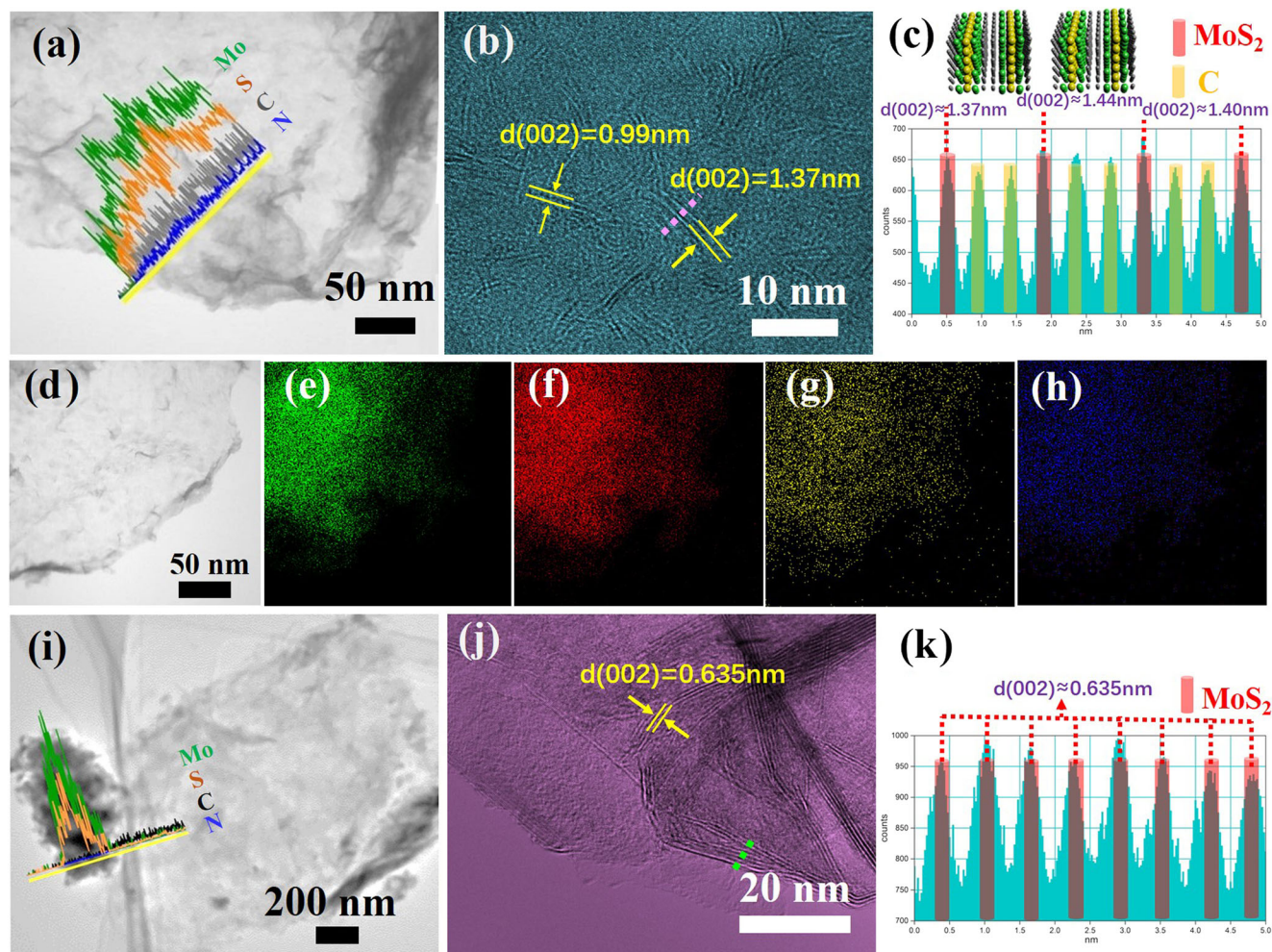


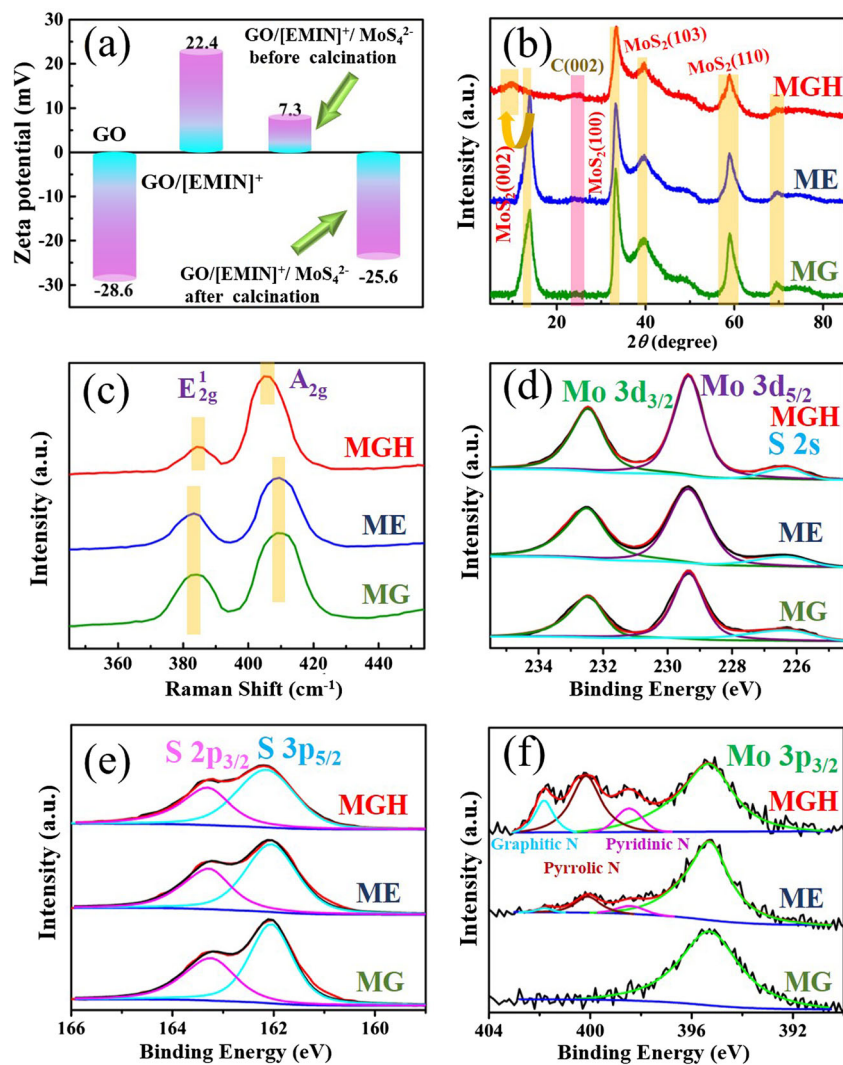
Fig. 2 **a** TEM image of MGH and EDX line scan profile of Mo (green), S (orange), C (gray), and N (blue). **b** High-resolution HRTEM image of MGH. **c** Line profiles of the d-spacing of the MoS₂ interlayers of MGH by the purple line in **b**. **d–h** Molybdenum, sulfur carbon, and nitrogen

elemental mapping of a selected area of MGH. **i** TEM image of MG and EDX line scan profile of Mo (green), S (orange), C (black), and N (blue). **j** High-resolution HRTEM image of MG. **k** Line profiles of the d-spacing of the MoS₂ interlayers of MG by the green line in **j**

Fig. 3f. Fitted high-resolution N 1s spectra indicate that the MGH is dominated by pyrrolic-type nitrogen (400.1 eV, 61.6%), comparison with pyridinic-type nitrogen (398.4 eV, 13.7%), and graphitic-type nitrogen (401.7 eV, 24.7%) in carbon materials. Therefore, by calculating the integral peak area of N and C, the nitrogen contents in carbon matrix are about 10.10%. Pyrrolic N not only possesses strong Na–N and S–N attraction but also maintains high electronic conductivity of carbon matrix [32]. Pyrrolic nitrogen-doped carbon can benefit Na⁺ diffusion and mitigate intermediate Na₂S/Na₂S_n [33]. The mass percentage of MoS₂ can be determined by the weight loss of TGA curves from 100 to 760 °C in air, related to the oxidation of MoS₂ and the combustion of carbon (Fig. S4). The retained weight percentages of MGH, MG, and ME maintain at 78.7, 85.6, and 83.1% in 760 °C, and the MoS₂ contents are calculated to be 89.4, 97.1, and 94.4%, respectively.

The electrochemical performances of MGH, ME, and MG were investigated using half cells versus Na/Na⁺ in Fig. 4. The capacity is calculated based on the total mass of the hybrid. The initial three CV curves of MGE are detailed in Fig. 4a at a sweep rate of 0.2 mV s⁻¹ between 0.01 and 3.0 V (Na vs. Na⁺). There are three obvious reduction peaks at 1.04, 0.49, and 0.19 V in the first cathodic sweep. The first cathodic peak at 1.04 V could be associated with the intercalation of Na⁺ in enlarged 2H-MoS₂ lattice to form 2H-Na_xMoS₂ (0 < x < 0.5) and the induced irreversible structural transition (2H-Na_xMoS₂ to 1T-Na_xMoS₂) [34]. The reduction peak at 0.48 V could be assigned to the decomposition of electrolyte and the formation of the solid electrolyte interphase (SEI) layer on the electrode surface, which dominates the major irreversible capacity loss in the initial cycle [35]. The peak below 0.19 V is attributed to decomposed reaction from 1T-Na_xMoS₂ to Na₂S and metallic Mo [36]. The broad oxidation

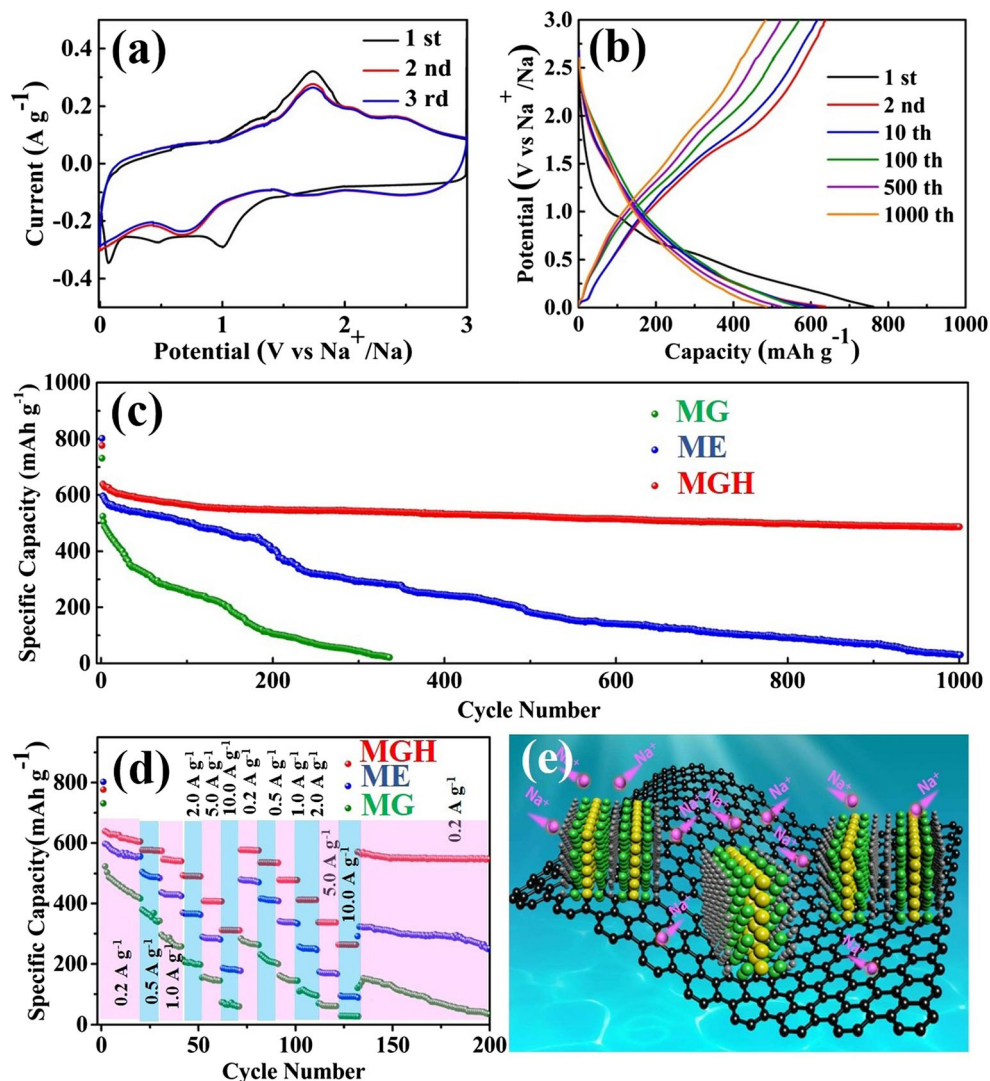
Fig. 3 **a** Zeta potentials of GO, GO via [EMIN]⁺, and GO/[EMIN]⁺/MoS₄²⁻ before and after calcination. **b** XRD patterns of MGH, MG, and ME. **c** The magnified Raman spectrum of the composites, showing the peaks of MGH, MG, and ME. **d** XPS S1s and Mo 3d spectrum of MGH, MG, and ME. **e** XPS S 2p spectrum of MGH, MG, and ME. **f** XPS N and Mo3p spectrum of MGH, MG, and ME



peak center at 1.75 V shows the conversion reaction of the metallic Mo nanograins reversing to MoS₂ [37]. The discharge/charge curves of MGH, ME, and MG are gained further insight into the reversibility of the electrodes. The following galvanotactic cycling profiles are almost overlapped, demonstrating excellent reversibility. A high initial discharge capacity about 776 mAh g⁻¹ is delivered with a high initial coulombic efficiency of 82.2%. The reversible discharge capacity of the MGE is 486 mAh g⁻¹, and the coulombic efficiency remains above 99% in the 1000th cycle. Unlike MGH, ME and MG presented undesirable capacity retention capability and reversibility shown in Fig. S5. Whereas the initial capacity of ME and MG are about 802 and 731 mAh g⁻¹ with a lower initial coulombic efficiency of 76.1 and 74.9%, respectively. The prominently superior reversibility and high initial coulombic efficiency of MGH can be ascribed to high material utilization from unique structure and the enhancement from nitrogen doped.

The long-term cycling performance of as-fabricated electrodes is listed in Figs. 4c and S6 for comparison. MGH could still reach the reversible capacity about 486 mAh g⁻¹ and capacity retention of 76.5% (based on the second cycle) after 1000 cycles, corresponding to a low fading capacity about 0.15 mAh g⁻¹ and fading cyclic rate of ca. 0.03% per cycle (Figs. 4c and S6a). In sharp contrast with MGE exhibiting superior long-term cyclability, ME delivers a gradually decreased reversible capacity merely remaining 31 mAh g⁻¹ after 1000 cycles (Figs. 4c and S6b), while MG shows an extremely lower capacity retention and rapidly decreases to 21 mAh g⁻¹ after 336 cycles (Figs. 4c and S6c). Another attractive property for MGH is its outstanding rate behavior. Detailed in Fig. 4d, the capacities of MGH at various current densities of 0.2, 0.5, 1.0, 2.0, 5.0, 10.0, 0.2, 0.5, 1.0, 2.0, 5.0, and 10.0 A g⁻¹ are 600, 574, 520, 463, 405, 330, 556, 505, 443, 379, 316, and 246 mAh g⁻¹, respectively. Compared with the MGH electrode, the ME and MG show lower rate capacity

Fig. 4 **a** CV curves of the first 3 cycles of the MGH electrode at scan rates of 0.2 mV s^{-1} as anode material for lithium ion battery. **b** The first three galvanostatic charge-discharge profiles of the MGH electrode at a current density of 0.2 A g^{-1} in the voltage range of $0.01\text{--}3.0 \text{ V vs. Na}^+/\text{Na}$. **c** Cycling performance of MGH, MG, and ME electrodes at a current density of 0.2 A g^{-1} . **d** Multi-rate testing of MGH, MG, and ME at discharge current densities of $0.2, 0.5, 1.0, 2.0, 5.0, 10.0, 0.2, 0.5, 1.0, 2.0, 5.0, 10.0,$ and 0.2 A g^{-1} . **e** Schematic of the electrolyte ion diffusion and fast electron transport in MGH



and rapider capacity decay. After the deep charge and discharge for 10 cycles at 10.0 A g^{-1} , the capacity of MGH can be covered and increased to 550 mAh g^{-1} , which it even remains very stable in extended rate cycling and performs excellent stability in the following cycles at 0.2 A g^{-1} .

As illustrated in Fig. 4e, the high reversible capacity, superior rate performance, and outstanding long-term durability could be ascribed to the unique vertically sandwiched structure and pyrrolic nitrogen-doped carbon, which can summarize as the following factors. First, flexible GO sheets service as a strain-relaxed conductive substrate for alleviating the MoS_2 aggregation or stacking/restacking in the long-term cycles. Second, vertical aligned monolayer MoS_2 with edge-terminated structure can facilitate electrical conductivity, shorten Na^+ diffusion paths, and migrate soluble polysulfide intermediate shuttling. These should be beneficial for minimized exposure of S atoms and maximized exposure of Van der Waals gaps. It is essential for excellent reversibility. Third, monolayer MoS_2 sandwiched by N-doped carbon layers

exhibits the large MoS_2/C heterogeneous interface areas. The improvement of electrochemical performance can be attributable to reasonable isolate MoS_2 phase, which ensures its structural stability against conversion reaction (1T-MoS_2 to metal Mo and Na_2S). Finally, pyrrolic nitrogen-doped carbon can enhance the surface adsorption of intermediate $\text{Na}_2\text{S}/\text{Na}_2\text{S}_n$, achieving stable long-term cycling [38]. Therefore, rational structure and pyrrolic nitrogen-incorporative enhancement synergistic effect achieves the electrochemical performance of the MGE anode.

Conclusions

In summary, we have designed and synthesized a novel MoS_2 -based hybrid via a facile ionic liquid-assisted reflux and annealing methods. In this hybrid, pyrrolic nitrogen-doped carbon sandwiches monolayer MoS_2 , and these hybrids vertically anchor on graphene oxides. Compared with the electrode

without ionic liquid-assisted synthesis, the hybrid electrode yields significant enhancement, especially in reversible capacity, rate performance, and capacity retention in the long cycles. This performance can be attributed to structural advantages and pyrrolic nitrogen modified. The as-prepared MoS₂/C-graphene hybrids exhibit an initial capacity up to 776 mAh g⁻¹ with a high first columbic efficiency of 82.2% for BILs at 200 mA g⁻¹. And, the electrodes display a high reversible capacity of 486 mAh g⁻¹ with a very low capacity decay of 0.15 mAh g⁻¹ per cycle at 0.2 A g⁻¹. Our work also provides an enlightening design and methodology for other related frontiers.

Acknowledgements The authors would like to acknowledge support from the National Natural Science Foundation of China (No. 51502057, 51572058, 51307046, 91216123, 51174063), the Natural Science Foundation of Heilongjiang Province (E201436), the International Science & Technology Cooperation Program of China (2013DFR10630, 2015DFE52770), Specialized Research Fund for the Doctoral Program of Higher Education (SRFDP 20132302110031), Natural Science Foundation of Heilongjiang Province of China (Grant No. E2016062), the China Postdoctoral Science Foundation (General Financial Grant No. 2014M561345), the Heilongjiang Postdoctoral Science Foundation (LBH-Z14105), the Scientific Research Foundation for the Returned Overseas Chinese Scholars of the State Education Ministry (No. 20151098), the University Nursing Program for Young Scholars with Creative Talents in Heilongjiang province (No. 2015082), the Open Project Program of the Key Laboratory for Photonic and Electric Band Gap Materials of the Ministry of Education of Harbin Normal University (No. PEBM201405), postdoctoral scientific research developmental fund of Henlongjiang Province (LBH-Q14144), the Research Foundation for the Returned Overseas Chinese excellent Scholars of Heilongjiang Province (No. 2015424), National Key Research & Development Program (2016YFB0303903), and the Foundation of Science and Technology on Advanced Composites in Special Environment Laboratory.

References

- Wen M, Liu X, Zhao Y, Liu S, Liu H, Dong Y, Kuang Q, Fan Q (2017) Synthesis of alluaudite-type Na₂VFe₂(PO₄)₃/C and its electrochemical performance as cathode material for sodium-ion battery. *J Solid State Electrochem* 22:891–898
- Hu X, Ji X, Yan M, Mai L, Hu P, Shan B, Huang Y (2015) Na⁺ intercalation pseudocapacitance in graphene-coupled titanium oxide enabling ultra-fast sodium storage and long-term cycling. *Nat Commun* 6:6929
- Hwang JY, Myung ST, Sun YK (2017) Sodium-ion batteries: present and future. *Chem Soc Rev* 46(12):3529–3614
- Guo YP, Wei YQ, Li HQ, Zhai TY (2017) Layer structured materials for advanced energy storage and conversion. *Small* 13(45):1701649
- Li L, Zhong B (2017) The design and preparation of the composite with layered spherical structure for Li-S battery. *J Solid State Electrochem* 22:591–598
- Xue Y, Zhang Q, Wang W, Cao H, Yang Q, Fu L (2017) Opening two-dimensional materials for energy conversion and storage: a concept. *Adv Energy Mater* 7(19):1602684
- Ma XX, Liu SK, Zhang K, Liu XS, Hao J, Chi CX, Zhao JP, Liu XX, Li Y (2018) Facile scalable synthesis of ordered macroporous few-layer MoS₂ and carbon hybrid nanoarchitectures with sodium-ion batteries. *J Mater Sci Mater Electron* 29(4):3492–3501
- Ma X, Liu X, Zhao J, Hao J, Chi C, Liu X, Yao L, Liu S, Zhang K (2016) Improved cycling stability of MoS₂-coated carbon nanotubes on graphene foam as a flexible anode for Lithium-ion batteries. *New J Chem* 41(2):588–593
- Wang X, Weng Q, Yang Y, Bando Y, Golberg D (2016) Hybrid two-dimensional materials in rechargeable battery applications and their microscopic mechanisms. *Chem Soc Rev* 45(15):4042–4073
- Luo C, Lin H, Qi R, Zhong N, Peng H (2017) High-performance supercapacitor electrode based on a nanocomposite of polyaniline and chemically exfoliated MoS₂ nanosheets. *J Solid State Electrochem* 21:2071–2077
- Wang T, Chen S, Pang H, Xue H, Yu Y (2017) MoS₂-based nanocomposites for electrochemical energy storage. *Adv Sci* 4(2):1600289
- Dou Y, Zhang L, Xu X, Sun Z, Liao T, Dou S (2017) Atomically thin non-layered nanomaterials for energy storage and conversion. *Chem Soc Rev* 46(23):7338–7373
- Kang W, Wang Y, Xu J (2017) Recent progress in layered metal dichalcogenide nanostructures as electrodes for high-performance sodium-ion batteries. *J Mater Chem A* 5(17):7667–7690
- Wang Z, Mi B (2017) Environmental applications of 2D molybdenum disulfide (MoS₂) Nanosheets. *Environ Sci Technol* 51(15):8229–8244
- Shan TT, Xin S, You Y, Cong HP, Yu SH, Manthiram A (2016) Combining nitrogen-doped graphene sheets and MoS₂: a unique film-foam-film structure for enhanced Lithium storage. *Angew Chem Int Edit* 55(41):12783–12788
- Lu Y, Zhao Q, Zhang N, Lei K, Li F, Chen J (2016) Facile spraying synthesis and high-performance sodium storage of mesoporous MoS₂/C microspheres. *Adv Funct Mater* 26(6):911–918
- Shi Z, Kang W, Xu J, Sun Y, Jiang M, Ng T, Xue H, Yu D, Zhang W, Lee C (2016) Hierarchical nanotubes assembled from MoS₂-carbon monolayer sandwiched superstructure nanosheets for high-performance sodium ion batteries. *Nano Energy* 22:27–37
- Oakes L, Carter R, Hanken T, Cohn AP, Share K, Schmidt B, Pint C (2016) Interface strain in vertically stacked two-dimensional heterostructured carbon-MoS₂ nanosheets controls electrochemical reactivity. *Nat Commun* 7:11796
- Stephenson T, Li Z, Olsen B, Mitlin D (2013) Lithium ion battery applications of molybdenum disulfide (MoS₂) nanocomposites. *Energy Environ Sci* 7(1):209–231
- Zhang K, Wang YM, Ma XX, Zhang HC, Hou S, Zhao J, Li XG, Qiang LS, Li Y (2017) Three dimensional molybdenum oxide/polyaniline hybrid nanosheet networks with outstanding optical and electrochemical properties. *New J Chem* 41(19):10872–10879
- Li H, Li W, Ma L, Chen W, Wang J (2009) Electrochemical lithiation/delithiation performances of 3D flowerlike MoS₂ powders prepared by ionic liquid assisted hydrothermal route. *J Alloys Compd* 471(1):442–447
- Teng Y, Zhao H, Zhang Z, Li Z, Xia Q, Zhang Y, Zhao L, Du X, Du Z, Lv P, Swierczek K (2016) MoS₂ nanosheets vertically grown on graphene sheets for lithium-ion battery anodes. *ACS Nano* 10(9):8526–8535
- Wu X, Xu X, Qi M, Li W, Bai J, Wang L (2013) Scalable synthesis of pyrrolic N-doped graphene by atmospheric pressure chemical vapor deposition and its terahertz response. *Carbon* 62:330–336
- Jiang H, Ren D, Wang H, Hu Y, Guo S, Yuan H, Hu P, Zhang L, Li C (2015) 2D monolayer MoS₂-carbon interoverlapped superstructure: engineering ideal atomic interface for lithium ion storage. *Adv Mater* 27(24):3687–3695
- Shi Y, Zhou W, Lu AY, Fang W, Lee Y, Hsu A, Kim S, Kim K, Yang H, Li L (2012) Van der Waals epitaxy of MoS₂ layers using graphene as growth templates. *Nano Lett* 12(6):2784–2791

26. David L, Bhandavat R, Singh G (2014) MoS₂/graphene composite paper for sodium-ion battery electrodes. *ACS Nano* 8(2):1759–1770
27. Ataca C, Topsakal M, Aktürk E, Ciraci S (2011) A comparative study of lattice dynamics of three- and two-dimensional MoS₂. *J Phys Chem C* 115(33):16354–16361
28. Li H, Zhang Q, Yap CCR, Tay BK, Edwin THT, Olivier A, Baillargeat D (2012) From bulk to monolayer MoS₂: evolution of Raman scattering. *Adv Funct Mater* 22(7):1385–1390
29. Huang X, Zeng Z, Zhang H (2013) Metal dichalcogenide nanosheets: preparation, properties and applications. *Chem Soc Rev* 44(5):1934–1946
30. Toth PS, Velický M, Bissett MA, Slater T, Savjani N, Rabiou A, Rakowski A, Brent J, Haigh S, O'Brien P (2016) Asymmetric MoS₂/graphene/metal sandwiches: preparation, characterization, and application. *Adv Mater* 28(37):8256–8264
31. Park J, Kim JS, Park JW, Nam T, Kim K, Ahn J, Wang G, Ahn H (2013) Discharge mechanism of MoS₂ for sodium ion battery: electrochemical measurements and characterization. *Electrochim Acta* 92(1):427–432
32. Zhao L, Hong C, Lin L, Wu H, Su Y, Zhang X, Liu A (2017) Controllable nanoscale engineering of vertically aligned MoS₂ ultrathin nanosheets by nitrogen doping of 3D graphene hydrogel for improved electrocatalytic hydrogen evolution. *Carbon* 116:223–231
33. Rao D, Wang Y, Zhang L, Yao S, Qian X, Xi X, Xiao K, Deng K, Shen X, Lu R (2016) Mechanism of polysulfide immobilization on defective graphene sheets with N-substitution. *Carbon* 110:207–214
34. González JR, Alcántara R, Tirado JL, Fielding A, Dryfe R (2017) Electrochemical interaction of few-layer molybdenum disulfide composites vs sodium: new insights on the reaction mechanism. *Chem Mater* 29(14):5886–5895
35. Zhang L, Tang Y, Wang Y, Duan Y, Xie D, Wu C, Cui L, Li Y, Ning X, Shan Z (2016) In situ TEM observing structural transitions of MoS₂ upon sodium insertion and extraction. *RSC Adv* 6(98):96035–96038
36. Li Q, Yao Z, Wu J, Mitra S, Hao S, Sahu T, Li Y, Wolverton C, Dravid V (2017) Intermediate phases in sodium intercalation into MoS₂ Nanosheets and their implications for sodium-ion batteries. *Nano Energy* 38:342–349
37. Ren W, Zhang H, Guan C, Cheng C (2017) Ultrathin MoS₂ nanosheets@metal organic framework-derived N-doped carbon nanowall arrays as sodium ion battery anode with superior cycling life and rate capability. *Adv Funct Mater* 27(32):1702116
38. Wang X, Li G, Seo M, Hassan F, Hoque M, Chen Z (2016) Sulfur atoms bridging few-layered MoS₂ with S-doped graphene enable highly robust anode for Lithium-ion batteries. *Adv Energy Mater* 5(23):1501106